
Graph Classification Gaussian Processes via Hodgelet Spectral Features

Mathieu Alain^{1,5,†} **So Takao**² **Bastian Rieck**³ **Xiaowen Dong**⁴ **Emmanuel Noutahi**⁵
¹University College London ²California Institute of Technology ³University of Fribourg
⁴University of Oxford ⁵Valence Labs
†mathieu.alain.21@ucl.ac.uk

Abstract

The problem of classifying graphs is ubiquitous in machine learning. While it is standard to apply graph neural networks for such tasks, Gaussian processes can also be used, by transforming graph features into the spectral domain, and using the resulting spectral features as input points. However, this approach only takes into account features on vertices, whereas some graph data also support features on edges. In this work, we present a Gaussian process-based classification algorithm that can utilise vertex and/or edges features to help classify graphs. Furthermore, we take advantage of the Hodge decomposition of vertex and edge features to increase the flexibility of the model, which can be beneficial on some tasks.

1 Introduction

Classification is omnipresent in machine learning, yet typically assumes the data to be Euclidean. Extending this task to non-Euclidean domains, such as graphs, is challenging due to their irregularity, varying sizes, and multi-site information (e.g. vertices and edges). However, classifying graphs is of critical importance in scientific and industrial applications, being used for instance to predict properties of molecules, or discovering new drugs [1, 2]. Graph neural networks [3] are usually the model of choice for such applications, however, a downside is that they may require large datasets to train. Gaussian processes (GP) [4], on the other hand, prove to be a data-efficient and interpretable modelling choice, not requiring validation sets to tune hyperparameters, while providing robust uncertainty estimates on predictions. This makes them well-suited for a range of situations, such as in small-data regimes and high-risk decision-making tasks that require reliable uncertainty estimates.

In a recent work, Opolka et al. [5] introduced a GP-based algorithm that is capable of classifying graphs. Their method relies on tools developed in the graph signal processing literature [6], such as the graph Fourier transform [7] and the spectral graph wavelet transform [8], to convert features in the graph domain into spectral features in the Euclidean domain. The latter can then be passed as input points to a GP, which is employed for classification via approximate inference [9]. More specifically, graph spectral methods provide a spectral representation of features on vertices. This representation is defined in the eigenspace of the graph Laplacian. Closely related are techniques developed in the early graph neural network literature, for instance Spectral Networks [10] and ChebNet [11], which rely on graph Fourier/wavelet transforms to define a notion of convolution on graphs.

While the method proposed in Opolka et al. [5] allows processing of features living on the vertices, it cannot straightforwardly take into account edge features. However, information about the edges of a graph can be as useful as the information on the vertices, for instance representing important quantities such as flows [12] and bond energies [13].

Our paper aims to fill this gap by proposing a GP-based classification algorithm that can naturally incorporate features on vertices, edges and, more generally, simplices, building on recent work defining GPs on simplicial complexes [14] and cellular complexes [15]. Furthermore, we utilise the celebrated *Hodge decomposition* on vertex, edges and simplices features. This splits the aforementioned eigenspace into three canonical subspaces, called *Hodge subspaces*, each with distinct properties. This enables the modelling of each component separately, using different kernels. This idea have been used successfully in past works [16–18, 14], allowing for greater model flexibility. To the best of our knowledge, we are not aware that these recent extensions and techniques have been applied in the context of graph classification. We demonstrate empirically that these extensions achieve similar or better performance than the GP-based method of Opolka et al. [5].

Finally, while we only consider graph data here, our method can be extended easily to higher-order networks, such as simplicial complexes, cellular complexes, and hypergraphs, that can describe polyadic interaction [19–22], generalising the dyadic interaction present in graphs (see Appendix C).

2 Gaussian Processes for Graph Classification

We assume a dataset containing M undirected graphs $\mathcal{G}^{(1)}, \dots, \mathcal{G}^{(M)}$ and labels $y^{(i)} \in \mathbb{Z}$, for $i = 1, \dots, M$. We give each graph an orientation and emphasise that this choice is arbitrary. Let $\mathcal{V}^{(i)}$ be the vertex set and $\mathcal{E}^{(i)}$ be the edge set, both finite. Each graph $\mathcal{G}^{(i)} = (\mathcal{V}^{(i)}, \mathcal{E}^{(i)})$ has $N_v^{(i)}$ vertices and $N_e^{(i)}$ edges, and an incidence matrix $\mathbf{B}_{ve}^{(i)} \in \mathbb{Z}^{N_v^{(i)} \times N_e^{(i)}}$. The latter encodes the incidence of each vertex with each edge, and furthermore defines the *graph Laplacian* $\mathbf{L}_v^{(i)} := \mathbf{B}_{ve}^{(i)} \mathbf{B}_{ve}^{(i)\top} \in \mathbb{Z}^{N_v^{(i)} \times N_v^{(i)}}$. By considering 3-cliques (see Appendix C.2), we obtain the edge-to-triangle incidence matrix $\mathbf{B}_{et}^{(i)} \in \mathbb{Z}^{N_e^{(i)} \times N_t^{(i)}}$, where $N_t^{(i)}$ is the number of triangles in $\mathcal{G}^{(i)}$. Likewise, we can define the *graph Helmholtzian* $\mathbf{L}_e^{(i)} := \mathbf{B}_{ve}^{(i)\top} \mathbf{B}_{ve}^{(i)} + \mathbf{B}_{et}^{(i)} \mathbf{B}_{et}^{(i)\top} \in \mathbb{Z}^{N_e^{(i)} \times N_e^{(i)}}$, which applies to edges rather than vertices. Let $\mathcal{V}^{(i)} \rightarrow \mathbb{R}^{D_v}$ and $\mathcal{E}^{(i)} \rightarrow \mathbb{R}^{D_e}$ be two functions defined on vertices and edges, respectively, for $D_v, D_e \in \mathbb{N}$. By introducing an ordering on vertices and edges, we can represent these functions trivially by the matrices $\mathbb{R}^{D_v \times N_v^{(i)}}$ and $\mathbb{R}^{D_e \times N_e^{(i)}}$, respectively. These are understood as vertex (and edge) feature matrices with D_v (and D_e) *channels*. We denote vertex features of channel $1 \leq d \leq D_v$ by the column vector $\mathbf{x}_{vd}^{(i)} \in \mathbb{R}^{N_v^{(i)}}$, and edge features of channel $1 \leq d \leq D_e$ by the column vector $\mathbf{x}_{ed}^{(i)} \in \mathbb{R}^{N_e^{(i)}}$. Note that graphs may have vertex features, edge features, or both.

2.1 Wavelet transforms on graphs

The key idea behind our graph classification algorithm is to convert vertex and edge features in the graph domain into spectral features in the Euclidean domain, enabling the use of standard GP classification using these transformed features. To this end, we first consider the eigendecomposition of the graph Laplacian and Helmholtzian

$$\mathbf{L}_v^{(i)} = \mathbf{U}_v^{(i)} \mathbf{\Lambda}_v^{(i)\top} \mathbf{U}_v^{(i)\top}, \quad \mathbf{L}_e^{(i)} = \mathbf{U}_e^{(i)} \mathbf{\Lambda}_e^{(i)} \mathbf{U}_e^{(i)\top}, \quad (1)$$

and define the *graph Fourier transform* as the projection of graph features onto the eigenbases,

$$\hat{\mathbf{x}}_{vd}^{(i)} := \mathbf{U}_v^{(i)\top} \mathbf{x}_{vd}^{(i)} \in \mathbb{R}^{N_v^{(i)}}, \quad \hat{\mathbf{x}}_{ed}^{(i)} := \mathbf{U}_e^{(i)\top} \mathbf{x}_{ed}^{(i)} \in \mathbb{R}^{N_e^{(i)}}. \quad (2)$$

Vertex and edge *Fourier coefficients*, respectively, $\hat{\mathbf{x}}_{vd}^{(i)}$ and $\hat{\mathbf{x}}_{ed}^{(i)}$, are invariant to vertex and edge ordering, making them sound choices for constructing spectral features. They capture *global* properties of the original features. However, it is often beneficial to use *spatially localised* information, i.e. focusing only on *local* neighbourhoods, and use a *multi-scale* resolution. A way to achieve this is to use the *graph wavelet transform* [8] (see Appendix B). *Wavelet functions*, $b : \mathbb{R} \rightarrow \mathbb{R}$ and $d : \mathbb{R} \rightarrow \mathbb{R}$, operate as band-pass filters, and consist of scaled and shifted variants of a *mother wavelet*. *Scaling functions*, $a : \mathbb{R} \rightarrow \mathbb{R}$ and $c : \mathbb{R} \rightarrow \mathbb{R}$, are low-pass filters. This yield the functions on eigenvalues,

$$w_{vj}(\lambda) := a(\alpha_j \lambda) + \sum_{l=1}^{L_v} b(\beta_l \lambda), \quad \Theta_{vj} := \{\alpha_j, \beta_1, \dots, \beta_{L_v}\}, \quad 1 \leq j \leq W_v, \quad (3)$$

$$w_{ej}(\lambda) := c(\gamma_j \lambda) + \sum_{l=1}^{L_e} d(\delta_l \lambda), \quad \Theta_{ej} := \{\gamma_j, \delta_1, \dots, \delta_{L_e}\}, \quad 1 \leq j \leq W_e, \quad (4)$$

where L_v, L_e are the number of *scales*, W_v, W_e the number of *filters*, and Θ_{vj}, Θ_{ej} are trainable parameters controlling the scales. Vertex and edge *wavelet coefficients* are given, respectively, by

$$\hat{\mathbf{x}}_{vdj}^{(i)} := \mathbf{U}_v^{(i)} w_{vj} (\mathbf{\Lambda}_v^{(i)}) \mathbf{U}_v^{(i)\top} \mathbf{x}_{vd}^{(i)} \in \mathbb{R}^{N_v^{(i)}}, \quad \hat{\mathbf{x}}_{edj}^{(i)} := \mathbf{U}_e^{(i)} w_{ej} (\mathbf{\Lambda}_e^{(i)}) \mathbf{U}_e^{(i)\top} \mathbf{x}_{ed}^{(i)} \in \mathbb{R}^{N_e^{(i)}}. \quad (5)$$

2.2 Hodge decomposition

The Hodge decomposition [23] (see Appendix C.3) states that vertex and edge features can be canonically decomposed into the sum of three orthogonal parts: *exact*, *co-exact*, and *harmonic*. This leads to breaking down the eigenbases according to the Hodge subspaces,

$$\mathbf{U}_v^{(i)} = [\mathbf{U}_{vc}^{(i)} \mathbf{U}_{vh}^{(i)}], \quad \mathbf{U}_e^{(i)} = [\mathbf{U}_{ee}^{(i)} \mathbf{U}_{ec}^{(i)} \mathbf{U}_{eh}^{(i)}]. \quad (6)$$

The co-exact eigenbasis $\mathbf{U}_{vc}^{(i)}$ corresponds to the non-zero eigenvectors of $\mathbf{L}_v^{(i)}$, and the harmonic eigenbasis $\mathbf{U}_{vh}^{(i)}$, the zero ones. The exact and co-exact eigenbases $\mathbf{U}_{ee}^{(i)}$ and $\mathbf{U}_{ec}^{(i)}$, respectively, are the non-zero eigenvectors of $\mathbf{B}_{ve}^{(i)\top} \mathbf{B}_{ve}^{(i)}$ and $\mathbf{B}_{et}^{(i)} \mathbf{B}_{et}^{(i)\top}$, respectively, and the harmonic eigenbasis $\mathbf{U}_{eh}^{(i)}$, the zero ones of $\mathbf{L}_e^{(i)}$.

2.3 Hodgelet spectral features

We generate spectral features from wavelet coefficients, and then use them in downstream GP classification tasks (see Appendix A). First, we take the wavelet transform (5) with respect to the decomposed eigenbasis $\mathbf{U}_v^{(i)}$ (6), yielding two wavelet coefficients, corresponding to the co-exact and harmonic parts. For every filter $1 \leq j \leq W_v$, and every channel $1 \leq d \leq D_v$, we concatenate the 2-norm of the coefficient $\hat{\mathbf{x}}_{vdj}^{(i)}$. This results in two column vectors $\mathbf{v}_c^{(i)}, \mathbf{v}_h^{(i)} \in \mathbb{R}^{W_v D_v}$, which we call vertex *Hodgelet spectral features*. We apply a similar procedure to get edge Hodgelet spectral features $\mathbf{e}_e^{(i)}, \mathbf{e}_c^{(i)}, \mathbf{e}_h^{(i)} \in \mathbb{R}^{W_e D_e}$. These are employed as input points for our additive *Hodgelet kernel*

$$\begin{aligned} \kappa(\mathcal{G}^{(i)}, \mathcal{G}^{(j)}) &:= \kappa_{vc}(\mathbf{v}_c^{(i)}, \mathbf{v}_c^{(j)}) + \kappa_{vh}(\mathbf{v}_h^{(i)}, \mathbf{v}_h^{(j)}) + \kappa_{ee}(\mathbf{e}_e^{(i)}, \mathbf{e}_e^{(j)}) \\ &+ \kappa_{ec}(\mathbf{e}_c^{(i)}, \mathbf{e}_c^{(j)}) + \kappa_{eh}(\mathbf{e}_h^{(i)}, \mathbf{e}_h^{(j)}), \end{aligned} \quad (7)$$

where each $\kappa_{\bullet\bullet}$ is a kernel, such as the squared exponential or Matérn kernel function. The $\Theta_{\bullet j}$ parameters are optimised jointly with the kernel hyperparameters.

3 Experiments

The aim of the experiments is two-fold: (1) we validate the added flexibility given by the Hodge decomposition, and (2) we demonstrate that when edge features are present, it is more beneficial to work with edges directly, rather than converting a graph to a line-graph.

The latter point has been observed in previous works, such as Schaub et al. [20] and Yang et al. [14], and our experiments further validate their conclusions.

3.1 Graph classification benchmarks

In our first experiment, we compare our method to Opolka et al. [5] on standard graph classification benchmark datasets that only contain vertex features. Specifically, we compare their algorithm, which we refer to the wavelet-transform GP (WT-GP), which does not use the Hodge decomposition, to our method, WT-GP-Hodge, which employs the decomposition. In Table 1, we display the results on some real and synthetic datasets used in Opolka et al. [5]. We observe that on all but one dataset (IMDB-BINARY), WT-GP-Hodge improves the classification accuracy. This may be surprising given that for vertex features, the Hodge decomposition only yields a co-exact and a harmonic part (since the exact part vanishes), and moreover, the harmonic part is just a constant value on the connected components of a graph. This implies that we can gain accuracy by splitting up vertex features into a constant bias (the harmonic part) and fluctuations around it (the co-exact part), and treating them separately with different kernels. However, when constant biases do not aid the classification, (e.g. when each class has vertex features of roughly equal magnitudes), then we do not expect WT-GP-Hodge to improve over WT-GP.

	ENZYMES	MUTAG	IMDB-BINARY	IMDB-MULTI	ring-vs-clique	sbm
WT-GP	65.00 \pm 4.94	86.73 \pm 4.18	74.20 \pm 3.87	48.73 \pm 2.76	99.5 \pm 1.5	86.42 \pm 6.92
WT-GP-Hodge	67.65 \pm 6.86	88.06 \pm 7.99	73.40 \pm 3.04	52.09 \pm 3.44	100.0 \pm 0.0	88.02 \pm 7.35

Table 1: Comparison of classification accuracy on several graph classification benchmark datasets. Results display means and standard deviations across 10 seeds.

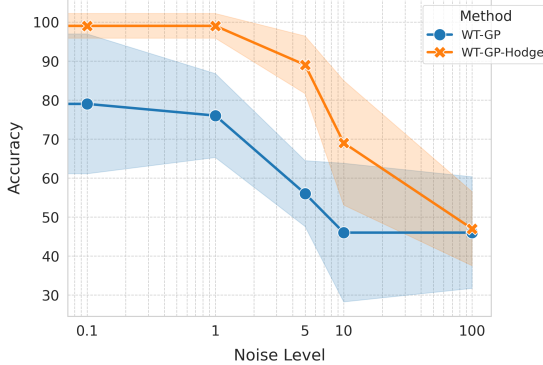


Figure 1: Accuracy vs. noise level in the vector field classification on 10 seeds.

N	WT-GP-LG	WT-GP-Hodge
25	51.0 \pm 16.4	50.0 \pm 14.1
50	53.0 \pm 17.9	73.0 \pm 12.7
75	56.0 \pm 14.3	85.0 \pm 12.8
100	54.0 \pm 15.0	89.0 \pm 10.4
150	57.0 \pm 13.5	92.0 \pm 7.0
200	54.0 \pm 12.0	94.0 \pm 8.0
250	58.0 \pm 16.6	95.0 \pm 7.2
300	56.0 \pm 12.8	93.5 \pm 7.8
350	53.0 \pm 13.3	94.8 \pm 7.4

Table 2: Accuracy of vector field classification. Results are across 10 seeds.

3.2 Vector field classification

In our second experiment, we consider the task of classifying noisy vector fields, i.e. predicting whether they are mostly divergence-free or curl-free. We proceed by generating 100 random vector fields, with half being mostly divergence-free (Figure D.1c), and the other half mostly curl-free (Figure D.1d). The generated vector fields are then projected onto the edges of a randomly generated triangular mesh on a square domain of N vertices (Figure D.2). Finally, we corrupt the edge features with i.i.d. Gaussian noise. The resulting dataset consists of 100 oriented graphs, each containing scalar edge features corresponding to the net flow of the vector field along the edges. Again, we compare our method against the vanilla WT-GP classification method. However, since WT-GP does not take edge features, when using this, we first convert the graph to a line-graph before applying it. We thus refer to it as WT-GP-LG. In Table 2, we display the results of WT-GP-LG and WT-GP-Hodge for various choices of N . We see that WT-GP-Hodge is consistently better, with large improvements as mesh resolution is increased. On the other hand, WT-GP-LG cannot distinguish accurately between divergence-free and curl-free fields, even as the mesh resolution becomes higher. Likely reasons for this are: (1) the Hodge decomposition in WT-GP-Hodge can help to distinguish more clearly between divergence-free and curl-free features, and (2) there are properties that are canonical to edges, such as orientation, which WT-GP-Hodge can handle naturally, whereas WT-GP-LG cannot. In Figure 1, we also plot the classification accuracy with varying noise level, which further shows robustness of WT-GP-Hodge to noise compared to WT-GP-LG.

4 Conclusion and Future Directions

We have presented a GP-based classification method that can classify graphs based on vertex and/or edge features. The vertex and edge features were processed by considering their projections onto the eigenbases of the graph Laplacian and Helmholtzian, respectively. The resulting wavelet coefficients were then used to construct wavelet spectral features, which were used as input points to a standard GP classification algorithm. Further, by taking the Hodge decomposition, we have shown that it can provide improvements over the method by Opolka et al. [5], even on graph data with only vertex features, owing to the added flexibility of the model. Overall, we have demonstrated the efficacy of our approach for graph classification tasks where edge features or topological information are essential. In the future, we intend to consider extensions to higher-order networks, such as simplicial complexes, cellular complexes, and hypergraphs, which we illustrate briefly in Appendix C.

Acknowledgments

MA is supported by a Mathematical Sciences Doctoral Training Partnership held by Prof. Helen Wilson, funded by the Engineering and Physical Sciences Research Council (EPSRC), under Project Reference EP/W523835/1. ST is supported by a Department of Defense Vannevar Bush Faculty Fellowship held by Prof. Andrew Stuart, and by the SciAI Center, funded by the Office of Naval Research (ONR), under Grant Number N00014-23-1-2729.

References

- [1] Xiao-Meng Zhang, Li Liang, Lin Liu, and Ming-Jing Tang. Graph neural networks and their current applications in bioinformatics. *Frontiers in Genetics*, 2021. (cited on page 1.)
- [2] Patrick Reiser, Marlen Neubert, André Eberhard, Luca Torresi, Chen Zhou, Chen Shao, Housam Metni, Clint van Hoesele, Henrik Schopmans, Timo Sommer, and Pascal Friederich. Graph neural networks for materials science and chemistry. *Communications Materials*, 2022. (cited on page 1.)
- [3] Franco Scarselli, Marco Gori, Ah Chung Tsoi, Markus Hagenbuchner, and Gabriele Monfardini. The graph neural network model. *IEEE Transactions on Neural Networks*, 2009. (cited on page 1.)
- [4] Carl Edward Rasmussen and Christopher K I Williams. *Gaussian processes for machine learning*. MIT Press, 2005. (cited on pages 1 and 7.)
- [5] Felix Opolka, Yin-Cong Zhi, Pietro Liò, and Xiaowen Dong. Graph classification gaussian processes via spectral features. In *Conference on Uncertainty in Artificial Intelligence*, 2023. (cited on pages 1, 2, 3, 4, and 10.)
- [6] Antonio Ortega, Pascal Frossard, Jelena Kovacëvić, José MF Moura, and Pierre Vandergheynst. Graph signal processing: Overview, challenges, and applications. *Proceedings of the IEEE*, 2018. (cited on page 1.)
- [7] David I Shuman, Sunil K. Narang, Pascal Frossard, Antonio Ortega, and Pierre Vandergheynst. The emerging field of signal processing on graphs: Extending high-dimensional data analysis to networks and other irregular domains. *IEEE Signal Processing Magazine*, 2013. (cited on page 1.)
- [8] David K Hammond, Pierre Vandergheynst, and Rémi Gribonval. Wavelets on graphs via spectral graph theory. *Applied and Computational Harmonic Analysis*, 2011. (cited on pages 1, 2, and 8.)
- [9] Hannes Nickisch and Carl Edward Rasmussen. Approximations for binary gaussian process classification. *Journal of Machine Learning Research*, 2008. (cited on page 1.)
- [10] Joan Bruna, Wojciech Zaremba, Arthur Szlam, and Yann LeCun. Spectral networks and locally connected networks on graphs. In *International Conference on Learning Representations*, 2014. (cited on page 1.)
- [11] Michaël Defferrard, Xavier Bresson, and Pierre Vandergheynst. Convolutional neural networks on graphs with fast localized spectral filtering. In *Conference on Neural Information Processing Systems*, 2016. (cited on page 1.)
- [12] Junteng Jia, Michael T Schaub, Santiago Segarra, and Austin R Benson. Graph-based semi-supervised and active learning for edge flows. In *International Conference on Knowledge Discovery and Data Mining*, 2019. (cited on page 1.)
- [13] Mingjian Wen, Samuel M Blau, Evan Walter Clark Spotte-Smith, Shyam Dwaraknath, and Kristin A Persson. Bondnet: a graph neural network for the prediction of bond dissociation energies for charged molecules. *Chemical Science*, 2021. (cited on page 1.)

- [14] Maosheng Yang, Viacheslav Borovitskiy, and Elvin Isufi. Hodge-compositional edge gaussian processes. In *International Conference on Artificial Intelligence and Statistics*, 2024. (cited on pages 2, 3, and 8.)
- [15] Mathieu Alain, So Takao, Brooks Paige, and Marc P Deisenroth. Gaussian processes on cellular complexes. In *International Conference on Machine Learning*, 2024. (cited on pages 2 and 8.)
- [16] Xiaoye Jiang, Lek-Heng Lim, Yuan Yao, and Yinyu Ye. Statistical ranking and combinatorial hodge theory. *Mathematical Programming*, 2011. (cited on page 2.)
- [17] Federica Baccini, Filippo Geraci, and Ginestra Bianconi. Weighted simplicial complexes and their representation power of higher-order network data and topology. *Physical Review E*, 2022. (cited on page 8.)
- [18] T Mitchell Roddenberry, Florian Frantzen, Michael T Schaub, and Segarra Santiago. Hodgelets: Localized spectral representations of flows on simplicial complexes. In *International Conference on Acoustics, Speech, and Signal Processing*, 2022. (cited on pages 2 and 8.)
- [19] Sergio Barbarossa and Stefania Sardellitti. Topological signal processing over simplicial complexes. *IEEE Transactions on Signal Processing*, 2020. (cited on page 2.)
- [20] Michael T Schaub, Yu Zhub, Jean-Baptiste Sebyc, T Mitchell Roddenberry, and Santiago Segarra. Signal processing on higher-order networks: Livin’ on the edge... and beyond. *Signal Processing*, 2021. (cited on pages 3 and 8.)
- [21] Theodore Papamarkou, Tolga Birdal, Michael Bronstein, Gunnar Carlsson, Justin Curry, Yue Gao, Mustafa Hajj, Roland Kwitt, Pietro Liò, Paolo Di Lorenzo, Vasileios Maroulas, Nina Milolane, Farzana Nasrin, Karthikeyan Natesan Ramamurthy, Bastian Rieck, Simone Scardapane, Michael T Schaub, Petar Veličković, Bei Wang, Yusu Wang, Guo-Wei Wei, and Ghada Zamzmi. Position: Topological deep learning is the new frontier for relational learning. In *International Conference on Machine Learning*, 2024. (cited on page 8.)
- [22] Claudio Battiloro, Lucia Testa, Lorenzo Giusti, Stefania Sardellitti, Paolo Di Lorenzo, and Sergio Barbarossa. Generalized simplicial attention neural networks. *IEEE Transactions on Signal and Information Processing over Networks*, 2024. (cited on pages 2 and 8.)
- [23] Lek-Heng Lim. Hodge laplacians on graphs. *SIAM Review*, 2020. (cited on page 3.)
- [24] Manfred Opper and Cédric Archambeau. The variational gaussian approximation revisited. *Neural Computation*, 2009. (cited on page 7.)
- [25] Yifan Feng, Haoxuan You, Zizhao Zhang, Rongrong Ji, and Yue Gao. Hypergraph neural networks. In *AAAI Conference on Artificial Intelligence*, 2019. (cited on page 8.)
- [26] Rubén Ballester, Ernst Röell, Daniel Bin Schmid, Mathieu Alain, Sergio Escalera, Carles Casacuberta, and Bastian Rieck. Mantra: The manifold triangulations assemblage, 2024. URL <https://arxiv.org/abs/2410.02392>. (cited on page 8.)
- [27] Ali Rahimi and Benjamin Recht. Random features for large-scale kernel machines. *Advances in neural information processing systems*, 20, 2007. (cited on page 10.)
- [28] Keenan Crane. Discrete differential geometry: An applied introduction. *Notices of the AMS, Communication*, 2018. (cited on page 10.)

A Gaussian Processes

Gaussian processes are stochastic processes that can be considered as Gaussian distributions extended to infinite dimensions. More precisely, a Gaussian process over \mathbb{R}^d is a random function $f : \Omega \times \mathbb{R}^d \rightarrow \mathbb{R}$, such that for any finite sequence of input points $\mathbf{x}_1, \dots, \mathbf{x}_M \in \mathbb{R}^d$, the random vector $[f(\mathbf{x}_1), \dots, f(\mathbf{x}_M)] \in \mathbb{R}^M$ is jointly Gaussian. Gaussian processes are defined by a mean function $\mu : \mathbb{R}^d \rightarrow \mathbb{R}$ and a kernel function $\kappa : \mathbb{R}^d \times \mathbb{R}^d \rightarrow \mathbb{R}$, which satisfy $\mu(\mathbf{x}) = \mathbb{E}[f(\mathbf{x})]$ and $\kappa(\mathbf{x}, \mathbf{x}') = \text{Cov}[f(\mathbf{x}), f(\mathbf{x}')]$, respectively, for any $\mathbf{x}, \mathbf{x}' \in \mathbb{R}^d$. We denote this relation by writing that $f \sim \text{GP}(\mu, \kappa)$. Gaussian processes are employed in the Bayesian inference paradigm: (1) a Gaussian process is defined as a prior on an unknown function, and (2) combined with a likelihood and training dataset, this produces a posterior process (not necessarily a Gaussian process). In the case of classification, the likelihood is non-Gaussian. For example, the Bernoulli likelihood is convenient for binary classification and, more generally, the categorical likelihood for multi-class classification. The ensuing posterior process is intractable and needs to be approximated, which can be done using *variational methods*.

For a complete presentation of Gaussian processes, we refer the reader to the book by Rasmussen and Williams [4].

A.1 Kernels

Gaussian process is uniquely characterised by a *mean function* and *kernel function*, which has the advantage of being simple and interpretable. The mean function is often taken to be zero (along a data normalisation), i.e. $\mu(\mathbf{x}) = 0$, for every $\mathbf{x} \in \mathbb{R}^d$, as it simplifies derivations and proofs. The kernel function is thus considered the most defining component in describing the behaviour of a Gaussian process and measures the similarities between two input points. It is important to note that a kernel function must be a *symmetric* and *positive semi-definite* function. Some popular choices are the square exponential kernel function (also called radial basis function kernel)

$$\kappa_{\text{se}}(\mathbf{x}, \mathbf{x}') := \sigma^2 \exp\left(-\frac{\|\mathbf{x} - \mathbf{x}'\|^2}{2\ell^2}\right), \quad \ell > 0, \quad (8)$$

and the Matérn kernel function

$$\kappa_{\text{mat}}(\mathbf{x}, \mathbf{x}') := \sigma^2 \frac{2^{1-\nu}}{\Gamma(\nu)} \left(\sqrt{2\nu} \frac{\|\mathbf{x} - \mathbf{x}'\|}{\ell}\right)^\nu K_\nu\left(\sqrt{2\nu} \frac{\|\mathbf{x} - \mathbf{x}'\|}{\ell}\right), \quad \ell, \nu > 0, \quad (9)$$

where $\|\cdot\|$ is the 2-norm, Γ the *gamma function*, and K_ν the *modified Bessel function* of the second kind. We observe that for $\nu \rightarrow \infty$, the Matérn kernel function converges to the square exponential kernel function.

A.2 Computational cost

Computing the posterior requires the inversion of a $N \times N$ *Gram matrix*, where N is the number of training input points. This results in a cubic computational complexity $\mathcal{O}(N^3)$ and quadratic memory requirements $\mathcal{O}(N^2)$. Fortunately, sparse Gaussian process [24] have been devised to alleviate this computational burden by constructing a smaller training dataset of M input points, called inducing points, where $M \ll N$.

B Wavelet Transforms

Spectral analysis is a set of tools for analysing and manipulating signals according to the eigenvalues, sometimes referred to as *frequencies*, of the Laplacian operator. The *Fourier transform* is the projection of signals onto the eigenvectors, called *Fourier basis*, of the Laplacian operator, thus producing *Fourier coefficients*. Although this provides a complete localisation in terms of frequency, it does not offer spatial localisation, and the resolution is fixed, i.e. it cannot capture localised changes in frequency. The *wavelet transform* provides both a balanced analysis between the spatial and spectral domains, and multi-scale resolution. The wavelet transform modulates the Fourier coefficients via *functional calculus* on the Laplacian operator. For graphs, this is done by applying a combination of two functions, a *wavelet function* and a *scaling function*, to the eigenvalues of the

graph Laplacian. A wavelet function is a scaled and shifted variant of a *mother wavelet*, acting as a band-pass filter, designed to cover medium and high frequencies. A scaling function acts as a low-pass filter, capturing low frequencies.

The reader is referred to Hammond et al. [8] for a detailed description of the graph wavelet transform.

B.1 Mother wavelet

A popular choice of mother wavelets is the Mexican hat wavelet, also called Ricker wavelet. The Mexican hat wavelet is defined as the negative normalised second derivative of a Gaussian function,

$$\phi(\lambda) := \frac{2}{\sqrt{3}\sigma\pi^{1/4}} \left(1 - \left(\frac{\lambda}{\sigma}\right)^2\right) e^{-\frac{\lambda^2}{2\sigma^2}}, \quad \sigma > 0. \quad (10)$$

C Extension to Higher-Order Networks

Graphs are one of the most versatile data structures. Indeed, vertices and edges can support signals, resulting in a richer structure than tabular data. Common examples are social networks, traffic maps, collaboration networks, and molecules. However, graphs do have their limitations: a graph only permits *dyadic interaction* between vertices via edges. Multiple recent works have tackle this issue by introducing more general structures, such as *simplicial complexes*, *cellular complexes* and hypergraphs [25, 20, 17, 18, 15, 14, 22, 21, 26].

C.1 Simplicial complexes

Simplicial complexes are an extension of graphs, and generalise the notion of triangles by using so-called *simplices* (*simplex* in the singular). In general setting, vertices are referred to as 0-simplices, and edges as 1-simplices. A 2-simplex is a triangle formed by three adjacent vertices. We observe that this describes a *triadic interaction* between vertices (a relation between three vertices). We can define simplices of arbitrary dimension $k \geq 0$. However, 0-, 1- and 2-simplices are sufficient in numerous interesting situations. A simplicial complex $\mathcal{S} = (\mathcal{V}, \mathcal{E}, \mathcal{T})$ is constructed from a vertex set \mathcal{V} , an edge set \mathcal{E} , and a triangle set \mathcal{T} . We say that \mathcal{S} is of dimension 2 and call it a simplicial 2-complex. Finally, the number of vertices, edges and triangles are denoted by N_v, N_e and N_t , respectively.

Orientation. So far, our simplicial complexes are *undirected*. We can give an *orientation* to a simplicial complex. An oriented simplicial 2-complex has an orientation on its edges and triangles, requiring an ordering to be imposed on its vertices. For an edge $e = \{v_1, v_2\}$, an orientation means assigning a direction, transforming e into (v_1, v_2) or (v_2, v_1) . We notice that an edge has always two possible orientations. Giving an orientation amounts to converting an undirected graph into a *directed* one. Likewise, a triangle $t = \{v_1, v_2, v_3\}$ has six possible orientations. However, two equivalence classes can be determined, reducing the orientation to be either *clockwise* or *anti-clockwise*. We point out that although an orientation is necessary to express concepts such as edge flows, the choice of orientation is arbitrary.

Cellular complexes. A more general structure is that of cellular complexes. The treatment of cellular complexes is similar to simplicial complexes. For more details, see Alain et al. [15]. For an illustration, we refer to Figure C.1. We could also easily handle hypergraphs by using a Laplacian on hypergraphs.

C.2 Hodge Laplacians

If one takes a step back, it becomes apparent that graphs and simplicial complexes have a *chain-like* structure: vertices are connected to edges, and edges are connected to triangles. More precisely, we say that vertices have edges as their *upper neighbours*, edges have vertices as their *lower neighbours* and triangles as their upper neighbours, and triangles have edges as their lower neighbours. This leads us to the definition of two incidence matrices, $\mathbf{B}_{ve} \in \mathbb{Z}^{N_v \times N_e}$ and $\mathbf{B}_2 \in \mathbb{Z}^{N_e \times N_t}$. While \mathbf{B}_{ve} is the incidence matrix between vertices and edges, \mathbf{B}_{et} is the incidence matrix between edges and triangles. In a general setting, these matrices are called *boundary matrices*, and are denoted by \mathbf{B}_1

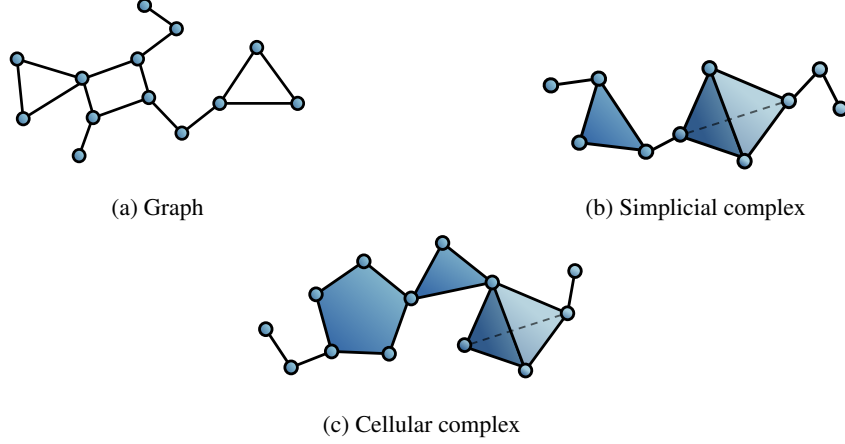


Figure C.1: Graph, simplicial complex, and cellular complex (specifically, a polyhedral complex). A simplicial complex cannot represent arbitrary polygons like the pentagon in (c).

and \mathbf{B}_2 , respectively, since vertices are 1-simplices, and edges are 2-simplices. This results in the general definition of a boundary matrix $\mathbf{B}_k \in \mathbb{Z}^{N_k \times N_{k+1}}$, where N_k is the number of k -simplices. Note that for a simplicial K -complex, $\mathbf{B}_0 = \mathbf{0}$ and $\mathbf{B}_{k+1} = \mathbf{0}$. For simplicial 2-complexes, it simply means that vertices have no lower neighbours, and triangles have no upper neighbours. We can define a more general notion of Laplacian, called the *Hodge Laplacian*,

$$\mathbf{L}_k := \mathbf{B}_k^\top \mathbf{B}_k + \mathbf{B}_{k+1} \mathbf{B}_{k+1}^\top \in \mathbb{Z}^{N_k \times N_k}. \quad (11)$$

The component $\mathbf{B}_k^\top \mathbf{B}_k$ is sometimes called the *lower Laplacian*, and $\mathbf{B}_{k+1} \mathbf{B}_{k+1}^\top$, the *upper Laplacian*. We observe that the graph Laplacian is nothing other than \mathbf{L}_0 , and the graph Helmholtzian is \mathbf{L}_1 .

Cliques. A k -clique is a subset of k vertices, such that every two (distinct) vertices in the clique are adjacent. In graphs, in other words, simplicial 1-complexes, edges have no upper neighbours. Hence, the edge-to-triangle incidence matrix $\mathbf{B}_2 = \mathbf{0}$. In turn, this implies that the graph Helmholtzian is equal to its lower Laplacian, i.e. $\mathbf{L}_1 = \mathbf{B}_1^\top \mathbf{B}_1$. However, it is possible to consider the 3-cliques of a graph in order to have a non-zero \mathbf{B}_2 . Intuitively, this is like considering triangles. We can then have a “full” graph Helmholtzian, i.e. $\mathbf{L}_1 = \mathbf{B}_1^\top \mathbf{B}_1 + \mathbf{B}_2 \mathbf{B}_2^\top$.

C.3 Hodge decomposition

The *Helmholtz decomposition*, a famous calculus theorem often called the fundamental theorem of vector calculus, states that any 2D vector fields on a Euclidean domain can be expressed as the sum of two orthogonal components: (1) one that intuitively has no sinks or sources, called *divergence-free* or *solenoidal*, and (2) one that has no vortices, also called *curl-free* or *irrotational*. This decomposition extended to differential forms on manifolds is referred to as the *Hodge decomposition*. In the case of Riemannian manifolds, we can identify differential 1-forms with vector fields, which results in a decomposition of vector fields on manifolds. The Hodge decomposition implies that the k -simplex feature space \mathbb{R}^{N_k} (for a single channel) can be decomposed into the sum of three orthogonal components: *exact*, *co-exact*, and *harmonic*. This leads us to the decomposition

$$\mathbb{R}^{N_k} = \text{im}(\mathbf{B}_{k+1}) \oplus \text{im}(\mathbf{B}_k^\top) \oplus \ker(\mathbf{L}_k), \quad (12)$$

where $\text{im}(\mathbf{B}_{k+1})$ is called the *exact subspace*, $\text{im}(\mathbf{B}_k^\top)$ the *co-exact subspace* and $\ker(\mathbf{L}_k)$ the *harmonic subspace*. Interestingly, we can see that the dimension of $\ker(\mathbf{L}_k)$ is equal to the k -th *Betti number*, which describe the number of k -dimensional holes. The Hodge decomposition implies the eigendecomposition of the Hodge Laplacian,

$$\mathbf{L}_k = \begin{pmatrix} \mathbf{U}_{ke} \\ \mathbf{U}_{kc} \\ \mathbf{U}_{kh} \end{pmatrix} \begin{pmatrix} \Lambda_{ke} & \mathbf{0} & \mathbf{0} \\ \mathbf{0} & \Lambda_{kc} & \mathbf{0} \\ \mathbf{0} & \mathbf{0} & \Lambda_{kh} \end{pmatrix} \begin{pmatrix} \mathbf{U}_{ke} \\ \mathbf{U}_{kc} \\ \mathbf{U}_{kh} \end{pmatrix}^\top, \quad (13)$$

where $(\Lambda_{ke}, \mathbf{U}_{ke})$ are the non-zero eigenvalues and eigenvectors of $\mathbf{B}_k^\top \mathbf{B}_k$, $(\Lambda_{kc}, \mathbf{U}_{kc})$ the non-zero eigenvalues and eigenvectors of $\mathbf{B}_{k+1} \mathbf{B}_{k+1}^\top$, and $(\Lambda_{kh}, \mathbf{U}_{kh})$ the zero eigenvalues and eigenvectors of \mathbf{L}_k . We observe that the *exact eigenbasis* $\mathbf{U}_{0e} = \mathbf{0}$, since $\mathbf{B}_0 = \mathbf{0}$. Similarly, *co-exact eigenbasis* $\mathbf{U}_{k+1e} = \mathbf{0}$, since $\mathbf{B}_{k+1} = \mathbf{0}$.

Hodgelet kernel. In the same spirit as Section 2.1, we define the wavelet transform on k -simplex features, obtain wavelet spectral features, and finally define the *Hodgelet kernel* on simplicial K -complexes,

$$\kappa(\mathcal{S}^{(i)}, \mathcal{S}^{(j)}) := \sum_{k=1}^K \left(\kappa_{ke}(\mathbf{s}_{ke}^{(i)}, \mathbf{s}_{ke}^{(j)}) + \kappa_{kc}(\mathbf{s}_{kc}^{(i)}, \mathbf{s}_{kc}^{(j)}) + \kappa_{kh}(\mathbf{s}_{kh}^{(i)}, \mathbf{s}_{kh}^{(j)}) \right). \quad (14)$$

D Experiment Details

D.1 Graph Classification Benchmarks

We refer to Opolka et al. [5] for details on all the datasets used in this section.

D.2 Vector Field Classification Details

We provide some details about the vector field classification experiment in Section 3. To generate a random vector field, we first sample a Gaussian process $f : \Omega \times \mathbb{R}^2 \rightarrow \mathbb{R}^2$, and then take its derivatives f_x, f_y in both spatial components. Noting that a curl-free 2D vector field is always the gradient of a potential, we can sample an arbitrary *curl-free field* by taking

$$\mathbf{X}_{\text{curl-free}} := \nabla f = [f_x, f_y]^\top. \quad (15)$$

Similarly, since a *divergence-free* 2D vector field is always a *Hamiltonian vector field*, we can choose

$$\mathbf{X}_{\text{div-free}} := \nabla^\perp f = [f_y, -f_x]^\top, \quad (16)$$

in order to sample an arbitrary divergence-free field.

For the vector field f , we used samples of the squared-exponential Gaussian process, sampled using its random feature approximation [27]. We display this in Figure D.1, where we plot the derivatives f_x, f_y , and their combinations to yield divergence-free and curl-free fields.

Our data consist of *mostly divergence-free and curl-free* vector fields, which are generated by considering the linear combination

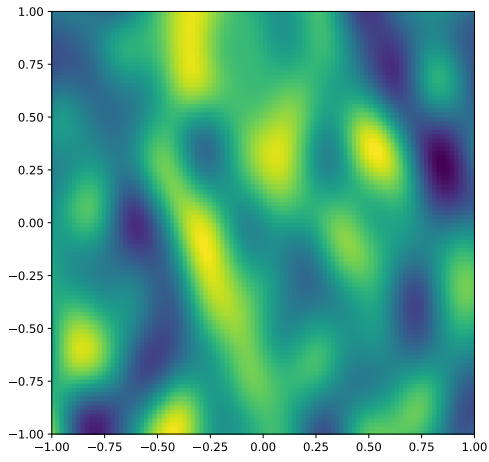
$$\mathbf{X} := \lambda \mathbf{X}_{\text{div-free}} + (1 - \lambda) \mathbf{X}_{\text{curl-free}} + R\epsilon, \quad (17)$$

where $\lambda \sim U([0.1, 0.5])$, $R > 0$ is the noise level, $\epsilon \sim \mathcal{N}(0, 1)$, and $\mathbf{X}_{\text{div-free}}, \mathbf{X}_{\text{curl-free}}$ generated randomly. If $\lambda < 0.5$, we say that the vector field \mathbf{X} is mostly curl-free, and if $\lambda > 0.5$, we say that it is mostly divergence-free.

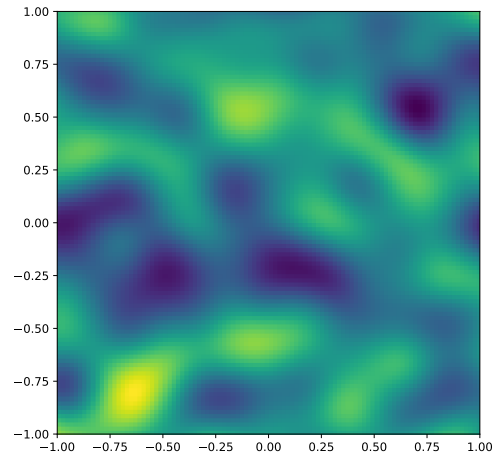
Projecting to a simplicial complex. To project a vector field $\mathbf{X} : \mathbb{R}^2 \rightarrow \mathbb{R}^2$ onto the edges of a graph, we employ the *de Rham map* [28], which “discretises” a vector field into edge signals. For a given edge $e = (v_0, v_1) \in \mathcal{E}$ with endpoint coordinates \mathbf{x}_0 and \mathbf{x}_1 , we define the projection X^e of \mathbf{X} onto e by the following integral,

$$X^e := \int_0^1 \mathbf{X}(\mathbf{x}_0 + t(\mathbf{x}_1 - \mathbf{x}_0)) \cdot \hat{\mathbf{t}} dt, \quad (18)$$

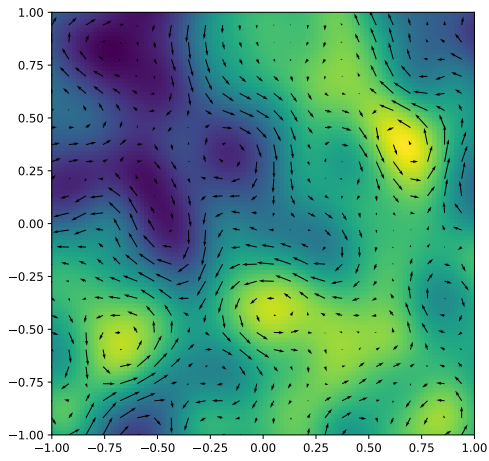
where $\hat{\mathbf{t}} := \frac{\mathbf{x}_1 - \mathbf{x}_0}{\|\mathbf{x}_1 - \mathbf{x}_0\|}$ is the unit tangent vector along the edge. Numerically, this can be computed efficiently using numerical quadratures, owing to the fact that the integral is only defined over the interval $[0, 1]$. Note that this depends on the ordering of the vertices v_0 and v_1 characterising the edge – if we flip the order, then the sign of X^e flips. Thus, we require the graph to be oriented in order for the projections $\{X^e\}_{e \in \mathcal{E}}$ to be well-defined. In Figure D.2, we display an example of such a projection onto a regular triangular mesh.



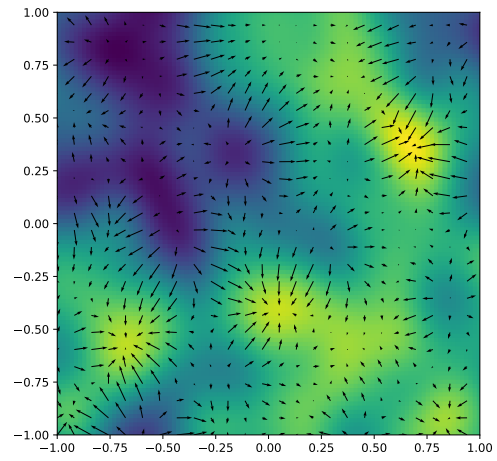
(a) Horizontal gradient f_x of a GP sample



(b) Vertical gradient f_y of a GP sample



(c) Divergence-free field $(f_y, -f_x)$



(d) Curl-free field (f_x, f_y)

Figure D.1: Illustration of the random vector field data generating process.

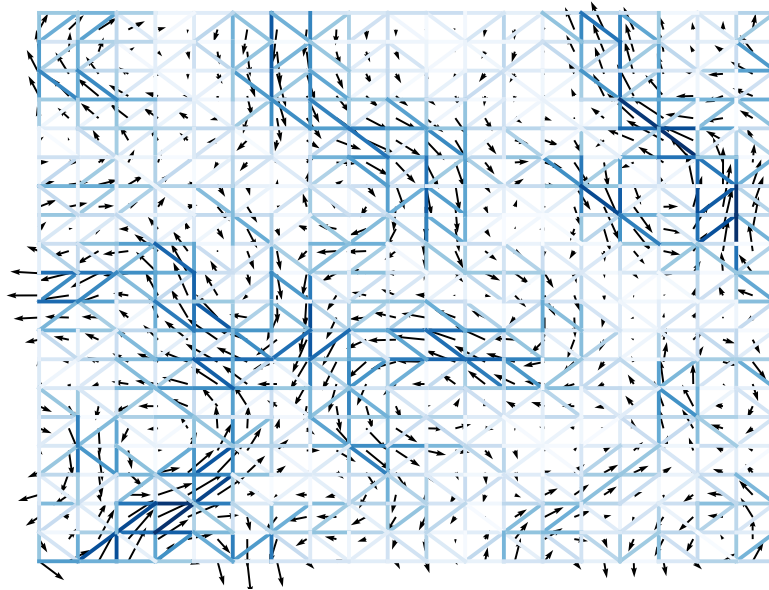


Figure D.2: Projection of a continuous divergence-free field onto a regular triangular mesh.